Journal of Fluids and Structures 17 (2003) 665–679

JOURNAL OF FLUIDS AND STRUCTURES

www.elsevier.nl/locate/jnlabr/yjfls

Flow pattern and velocity field distribution of cross-flow around four cylinders in a square configuration at a low Reynolds number

K. Lam[a,*], J.Y. Li[b], K.T. Chan[a], R.M.C. So[a]

[a] *Department of Mechanical Engineering, The Hong Kong Polytechnic University, Hung Hom, Kowloon, Hong Kong*
[b] *Department of Fluid Engineering, Xi'an Jiaotong University, Shaanxi, People's Republic of China*

Received 13 February 2002; accepted 28 November 2002

Abstract

The flow around four cylinders in a square configuration with a spacing ratio of 4 and at a Reynolds number of 200 were investigated using laser-induced fluorescence (LIF) visualization and particle image velocimetry (PIV) for angles of incidence ranging from $\alpha = 0^\circ$ to 45° at a 5° interval. Several distinct flow patterns were observed. Dependent on α, the flow was classified into three basic flow regimes. Each regime has its own dominant flow pattern and could lead to different problems. Two distinct flow patterns, which could lead to strong flow-induced vibration, were observed in this experiment. One is the impingement of oncoming vortices on the cylinders directly. The other is the formation of a jet flow between the near wake (or alternatively known as stagnation wake) of the upstream cylinder and downstream cylinder and such a jet flow is most prominent at $\alpha = 15^\circ$. These experimental results can be used to validate numerical simulation methods developed to investigate flows around cylinder arrays.

1. Introduction

Cross-flow around a group of cylinders is very common in engineering. Examples include offshore structure platforms, overhead cables, heat exchanger and steam boiler tube arrays. As a result of the variation of the spacing ratio, T/d, and orientation of the structural arrays cited above, the interaction of adjacent structures in these arrays would greatly affect the flow patterns around the structures. Here, T is the separation distance between two structures, measured between their geometric centers, and d is their hydraulic diameter. The changes include main flow direction, vortex-shedding, near-wake flow patterns, the positions of boundary layer separation, the stagnation regions, and the local velocity distributions. As a classical problem in fluid mechanics, cross-flow around a group of circular cylinders, which can be used to idealize structural arrays, could exhibit many interesting and unexpected phenomena due to the effect of mutual interference. Numerous studies have concentrated on the effects of interference between two, three, and four cylinders in laminar and turbulent flows. In reviewing a number of investigations concerning mutual interference, Zdravkovich (1987) proposed to classify the flow interference into three categories. These are proximity interference P, wake interference W, and a combination of P and W.

Experiments on cross-flow around two cylinders have been widely carried out. To cite a few examples, Bearman and Wadcock (1973) studied the deflected gap flow between two side-by-side circular cylinders and highlighted the bi-stable

*Corresponding author..
E-mail address: mmklam@polyu.edu.hk (K. Lam).

0889-9746/03/$ - see front matter
doi:10.1016/S0889-9746(03)00005-7

flow pattern in the flopping regime. They measured the base pressure C_{pb} at Re = 25 000. The Reynolds number Re is defined with respect to the free stream velocity U_0 and d. At $T/d = 1.1-2.0$, the base pressure was found to change from one steady value to another or flop between the two extremes. Meanwhile, Price and Paidoussis (1984) measured the aerodynamic forces acting on groups of two and three circular cylinders. Using pressure measurements and flow visualization, Gu (1996) and Gu and Sun (1999) studied the interference between two circular cylinders at high subcritical and supercritical Re. They further extended the classification of Zdravkovich (1987) to wake interference, shear layer interference and neighborhood interference. Sumner et al. (1999) studied the wake of two and three side-by-side circular cylinders in a range of $T/d = 1-6$ with Re = 500−3000 using flow visualization, hot film anemometry and particle image velocimetry. In their studies, the near-wake flow patterns were obtained. For the two cylinder arrangements, three basic flow patterns, i.e., a single vortex street flow, a deflected gap flow and a symmetric, equal-sized and synchronized vortex-shedding near-wake flow, were observed as T/d increased. In the wakes of the three side-by-side cylinders, both symmetric and asymmetric biased flow patterns were observed at $T/d = 1.25$, whereas only a symmetric biased flow pattern was found at $T/d = 1.5$. Furthermore, using flow visualization and particle image velocimetry (PIV) techniques, Sumner et al. (2000) systematically investigated the flow patterns around two circular cylinders of equal diameter for T/d ranging from 1.0 to 5.0 and an angle of incidence, $\alpha = 0-90^\circ$. Careful examination of the results revealed nine refined flow patterns and new insight was gained concerning the Strouhal number, St. Apart from the studies on two rigidly mounted cylinders at fixed positions, investigations on the fluid elastic forces and the mechanism of galloping interference have also been carried out (Ruscheweyh, 1983; Dielen and Ruscheweyh, 1995; Ting et al., 1998). In addition, numerical studies on a pair of side-by-side circular cylinders (So et al., 2000; Liu et al., 2001; Ng and Ko, 1995) have been conducted.

On the other hand, investigations on three- and four-cylinder arrays have been relatively scarce. Most of the studies were on flow around two-, three- and four-cylinder arrays in a side-by-side configuration and the emphases were on the flopping regime, such as that reported by Guillaume and LaRue (1999). However, a few studies on a group of three cylinders have revealed some new features. For example, Zdravkovich (1968) conducted a smoke visualization study of the laminar wake with Re = 60−300 behind three cylinders in various triangular configurations. The coexistence of multiple Karman vortex streets was observed. The vortices decayed very quickly and an entirely new single vortex street was formed. A more detailed study by Lam and Cheung (1988) using flow visualization revealed other prominent features of the flow pattern and vortex shedding from three cylinders in different equilateral arrangements. Their results showed that the well-known bi-stable biased flow behind two side-by-side cylinders and flow symmetry around two cylinders in tandem are suppressed or changed by the presence of the third cylinder at some specified configurations. Another example is the slightly staggered inverted-T arrangement, which means that one cylinder is placed upstream with two downstream cylinders slightly staggered. Under this arrangement, the wake behind the front cylinder is not narrow and the corresponding wake behind the downstream cylinder is not wide. From this experiment, it is obvious that the flow pattern of three cylinders in triangular configuration is quite different from that of two-, three- or four-cylinder arrays in a side-by-side arrangement. This is because of the presence of a third cylinder placed either upstream or downstream of the two-cylinder arrangement.

Experiments on other aspects of three-cylinder arrays have also been carried out. For example, using a pneumatic averaging manifold system, Kareem et al. (1998) investigated the interaction of two and three cylinders in line as well as three cylinders in an inverse-T and T arrangement in a boundary layer flow. Tatsuno et al. (1998) investigated the force acting on three cylinders in an equilateral arrangement and their interactions using pressure measurements, and found different flow patterns at some specific configurations.

Although the equidistant square arrangement of four cylinders is a fundamental arrangement, investigation on the flow around them is rather scarce and has not been well documented in the literature. Sayers (1988, 1990) conducted experiments on four cylinders in a square configuration at Re = 30 000 and in the T/d range of $1.1–1.5 < T/d < 5$. He measured the base pressure using an inclined alcohol manometer, the vortex shedding using a hot-wire anemometer, while the lift coefficient C_L and the drag coefficient C_D acting on one of the cylinders were obtained by integrating the measured pressure distribution around the cylinder. In his studies, it was found that the magnitude of C_L and C_D is strongly influenced by the orientation of the array group to the free stream. At certain spacing ratios and flow inclination angles, asymmetrical vortex shedding occurs, while in other situations, vortex shedding may be completely absent. Furthermore, a small change in the direction of the free stream could result in a large change in the vortex-shedding frequency. The visualization study of Lam and Lo (1992) clearly revealed the reason of the change of the vortex-shedding frequency in the study of Sayers (1990). They showed that the wake around the four cylinders in a square configuration is far more complicated than that in one or two cylinders. Moreover, Lam and Fang (1995) measured in detail the pressure distributions around the four cylinders. On the other hand, Farrant et al. (2000) carried out a numerical investigation on the flow around four cylinders in a square configuration using cell boundary element method.

As pointed out by Sumner et al. (2000), determining the fluid behavior from measured quantities is prone to misinterpretation, particularly when it is carried out without the benefit of flow visualization. Therefore, flow visualization is a very useful approach to gain understanding of the fluid dynamics and flow pattern of multiple cylinders in a cross-flow. However, up to now, information on the full field velocity distribution and the flow visualization of the flow patterns at low Re around four cylinders in a square configuration are still not available. Therefore, a number of questions have yet to be answered. How is the velocity field distributed in relation to the complex flow patterns? Where is the location of maximum velocity and why does it form there? What is the influence of the change of velocity on the fluctuating forces acting on the cylinders? How would the flow patterns be affected by the presence of other cylinders? In order to answer some of these questions, a detailed investigation of the instantaneous velocity field using PIV was conducted. This investigation would give the velocity maps of the flow. Furthermore, laser-induced fluorescent (LIF) was used to provide a clear picture of the evolution of the flow patterns and their vortex interactions. It is hoped that the studies could provide important information and understanding of the physics of this cross-flow around a cylinder array as well as some database to validate computational fluid dynamics (CFD) codes. In this paper, as a first attempt, the flow patterns and flow fields of the four cylinders in a square configuration at $\mathrm{Re} = 200$ and $T/d = 4$ were investigated.

2. Experimental setup and procedures

The experiments were carried out in a low-speed closed-loop water tunnel with a square working section of 150×150 mm. The walls of the test-section were made of acrylic and glass plates to facilitate laser transmission and flow visualization. The investigations were conducted at $\mathrm{Re} = 200$.

All four cylinders were installed on a circular vertical turntable in a cantilever manner, and the clearance between the ends of the cylinders and the sidewall of the test-section was ~ 1 mm. A schematic of the array configuration is shown in Fig. 1. Note the numbering of the cylinders and the angle of attack α is measured with respect to the line joining cylinders 1 and 4. Mounting facilities were provided in one of the vertical walls at the measuring station so that the plate can be flush mounted with the surface of the wall and can be rotated to any desired angle α. The cylinder cluster was always positioned in the middle of the working section to lessen near-wall effects and α was varied from 0° to 45° in 5° increments.

In the PIV experiments, the cylinder models were made of hollow glass tubes filled with water. This was carried out to minimize the shadow created by the cylinders when illuminated by a laser sheet, so that the interstitial flow velocity field can be measured. One end of each cylinder was sealed with a cap to prevent leakage while the other end was fitted with an adapter cap. The adapter cap was specially designed so that one of its ends could be fitted securely into the remaining open end of the cylinder while the other end went through the plate and was tightened up by nuts from the other side. The outer diameter of the cylinder is $d = 10$ mm. This leads to an aspect ratio of about 15 and a blockage ratio (per cylinder) of $\sim 6.7\%$. In order to facilitate the use of the PIV technique, nearly neutrally buoyant reflective tracer particles of diameter 50 μm in size were added to the recirculating water tunnel system as shown in Fig. 2. The mid-section of the cylinder array was illuminated with a scanning light sheet generated by a 4W Spectra-Physics Stabilite 2017 argon-ion laser. A scanner controller was used to control the scanning frequency of the light sheet with a range from 1.5 to 12.5 ms. The digital images were recorded using an Adimec MX12P CCD camera and a Matrox Pulsar

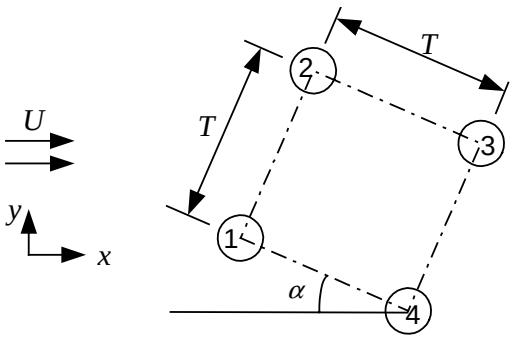

Fig. 1. A general configuration of the four-cylinder model.

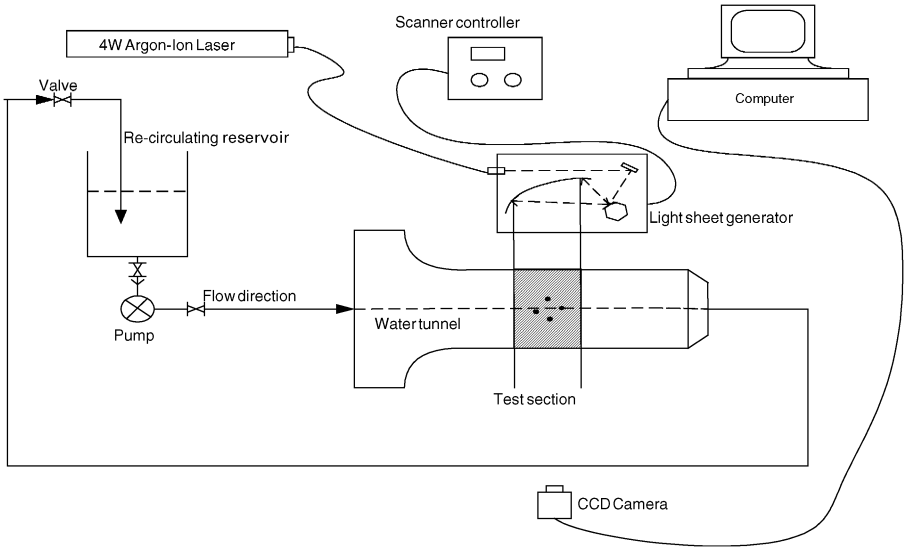

Fig. 2. A schematic diagram of the water tunnel and the set up of the PIV system.

frame grabber. The resolution of the camera is 1024×1024 pixels, while the integration time can be varied from 2 to 38 ms so that the speed is fast enough to provide a single frame/multi-exposed image. A maximum frame rate of about 25 images/s could be taken so that the cross-correlation technique of the multi-frame/single exposure method can be performed. The size of the imaging area covered about 120 mm × 120 mm of the flow region. The camera data transfer interface was installed in a Pentium III 600 MHz computer with a high-resolution monitor of the same order as the pixel density, a 256 Mbytes RAM and a 10 Gbyte hard disk.

Once the CCD camera has captured the digital image of the flow field, optical flow system software (VidPIV) was used to carry out the auto-correlation or cross-correlation analysis to deduce the vector field. In the analysis, the image is divided into small "interrogation region". The interrogation window is 32×32 pixels, corresponding to a flow area of about 3.75 mm × 3.75 mm. The image magnification was of the order of 0.117 mm/pixel, so in a 40 ms time difference (25 frames/s) between the images comprising a pair, a particle moving at the mainstream velocity of 20 mm/s ($Re = 200$) would cover a distance of 0.8 mm, i.e., 6.8 pixels or $0.08d$. Of course, the size of the interrogation window effectively limits the size of the vortex structures captured. After the image fields have been digitized, the particle displacements are extracted using a cross-correlation algorithm. In evaluating the cross-correlation, the initial positions of the seeding particle images were recorded on the first frame and the final positions were recorded on the second frame. The displacements of the seeding particles between the first frame and the second frame over the time interval were used to determine the velocity vectors. From the velocity plot, the streamline pattern and the vorticity map can be drawn. The measurement uncertainty of the velocity and the vorticity was conservatively estimated at 15%.

In the LIF flow visualization experiments, to ensure the transparency and smoothness of the cylinders, the Plexiglas cylinder models with $d = 10$ mm were machined and polished so that laser light can penetrate through the smooth circular cylinders. All the cylinders were installed on the same plate using the same method as before, this gave rise to the same aspect ratio and blockage as those in the PIV experiments. Each cylinder has two dye injection holes of 0.5 mm located at mid-span and on opposite side of the tube. The dye streak lines were illuminated using the same laser sheet and recorded with a JVC GY-DV500 Camcorder. The shutter speed used in this experiment was 1/250 s, which was fast enough to freeze the flow pattern of the streak line. The video results were first recorded in mini digital videocassette for about 7–20 min. After analyzing the video results by playing it on a computer monitor, some typical clips were transferred to a PC computer using Adobe Premiere 5.0 software and instantaneous photos could be obtained. The movie capture card is a DV500 card installed in a PC III computer with a 256 Mbytes RAM and a 30 Gbyte hard disk.

Two types of fluorescent dyes, rhodamine and fluorescein, were injected into the cylinders and then released into the main flow. Under the illumination of an argon-ion laser, LIF would occur. The fluorescent colors of rhodamine and fluorescein were brilliant yellow and green respectively. In the experiments, the Rhodamine dye was injected into cylinders 1 and 2, while fluorescein was used in cylinders 3 and 4. Therefore, the different flow patterns were easily recognized and the mutual interaction could be examined. Studying the video playback and comparing with still camera photos, a more detailed description of the flow pattern and its mechanism could be developed.

3. Results and discussion

In this experiment, the angle of rotation is clockwise at a 5° interval, so cylinder 2 is in the highest position when $\alpha = 45°$. Altogether, 10 sets of results were obtained; they ranged from $\alpha = 0-45°$. The diffusivity of the dye in the LIF visualizations is very low; therefore, they could faithfully follow the motion of the fluid particle and give a fairly detailed picture of the vortex structures and their development once they are entrained into the vortex structure. However, it should be noted that the dye filaments shown in the visualization results represent streak lines that contain flow history integrated all the way back to the point at which the dye is introduced into the flow. Furthermore, streak line, path line and streamline are identical only under steady flow conditions. On the other hand, PIV results can supply quantitative flow information about the velocity field, the vorticity map and streamlines. Therefore, a comparison of these two kinds of flow visualization results could lead to an understanding of the vortex dynamics and the mechanics of cross-flow around the four-cylinder array.

Depending on α, the overall flow patterns show four distinctive features. In order to provide a systematic and concise description of these experiments, the results are organized into four distinctive groups. The first group is given by the fundamental flow pattern obtained at $\alpha = 0^o$ and the results for this configuration are given in Figs. 3 and 4. The second group, designated here as the Opposite Vortex Squeezing and Absorbing flow pattern (OVSA), is given by the configuration covering an α range from 5° to 15°. The representative pattern at $\alpha = 15°$ is shown in Figs. 5 and 6. A third representative group, denoted as VPRP flow pattern (VPRP), occurs in the α range, 20–35° and the results at $\alpha = 30°$ are given in Figs. 7 and 8. Finally, the fourth representative group, designated as vortex impingement (VI) and induced separation (VIIS) flow pattern, is found in the α range, 40–45°. The results obtained at $\alpha = 45°$ are shown in Figs. 9 and 10.

All 10 sets of results are for the case where the free stream velocity is 20 mm/s, or $Re = 200$. The results shown in Figs. 3–10 were deduced from the digital video and the PIV measurements. For each α, the flow visualization results are presented in a figure with six sequential photos to demonstrate a complete vortex-shedding cycle. In the LIF sequential figure, τ is the periodic time period and t is the instantaneous time. The PIV results are shown in a separate figure with three different panels arranged from left to right to give the velocity vector plot, the streamline pattern and the vorticity map. In the velocity field map, a velocity vector scale corresponding to 100 mm/s is inserted for comparison. In the vorticity map, the minimum contour level is $1\,s^{-1}$ and the contour increment is $1\,s^{-1}$, solid lines represent positive contours, while negative contours are shown as dash lines.

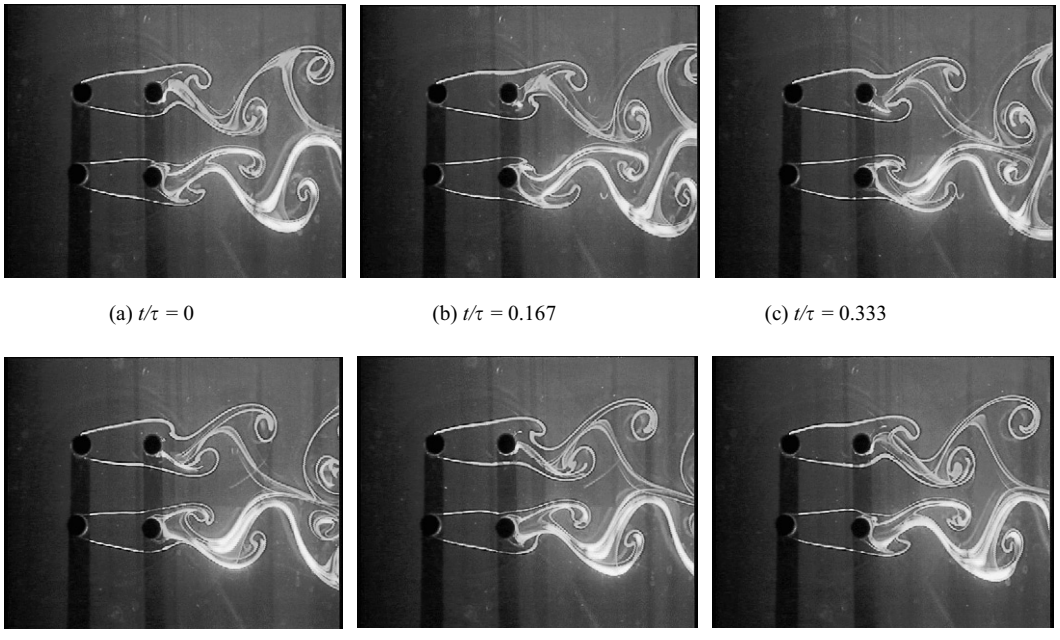

(a) $t/\tau = 0$ (b) $t/\tau = 0.167$ (c) $t/\tau = 0.333$

(d) $t/\tau = 0.5$ (e) $t/\tau = 0.667$ (f) $t/\tau = 0.833$

Fig. 3. Sequential photos of flow visualization at $\alpha = 0°$.

3.1. Fundamental flow pattern—in-line square configuration

At $\alpha = 0^\circ$, the cylinder array is an in-line square arrangement, and it can be regarded as two side-by-side rows of two-cylinder array in tandem. Six representative sequential photos of the flow patterns are shown in Fig. 3. In these photos, it is clearly observed that the downstream cylinders 3 and 4 are completely shielded by their corresponding upstream cylinders 1 and 2. No vortex shedding occurs for the upstream cylinders and the shear layers of cylinders 1 and 2 grow into mature vortices only after they have reached the rear side of cylinders 3 and 4. The positions of their boundary layer separation are observed to be similar to that for a single cylinder, which is after the pressure minimum point. On the other hand, vortices are shed immediately downstream of cylinders 3 and 4. Unlike two side-by-side cylinders, the shear layers of cylinders 1 and 2 are rather unstable. Often the inner shear layer of cylinder 2 would touch cylinder 3 instead of the corresponding layer of cylinder 1 on cylinder 4. Sometimes the shear layers of cylinder 2 became so wide that even the upper shear layer of cylinder 1 was pushed to flow below the contour of cylinder 4. Furthermore, the outer shear layers of cylinders 1 and 2 normally move obliquely outwards symmetrically to some extent. The presence of the second row of cylinders causes the shape of the shear layers of the individual cylinder to be different from those observed in a two side-by-side cylinder array at $T/D = 4$.

Comparing photo (a) with photo (d) in Fig. 3, it can be seen that the flow near cylinders 3 and 4 oscillates as a result of the influence of the wake of cylinders 1 and 2. Therefore, the lift and drag fluctuating forces on cylinders 3 and 4 would be larger than those on cylinders 1 and 2. Moreover, the drag force acting on cylinders 1 and 2 should be much larger than that on the downstream cylinders since cylinders 3 and 4 are completely shielded by the upstream cylinders. The deduction on the forces from the LIF flow results was verified in another experiment using a single load cell to measure the dynamic force acting on the cylinder. (This latter result is currently under preparation for publication.) The force measurement experiments were carried out in a closed-loop wind tunnel with a cross-section of 0.6 m × 0.6 m and a $T/d = 3.83$, which was similar to that used in this experiment. The diameter of the brass tube is 35 mm and the Re varies from 22 000 to 48 000. The deduction is also supported by the experiment of Lam and Fang (1995) at $\mathrm{Re} = 12\,800$, where pressure transducer was used to measure the surface pressure and hence the force.

Normally, for two cylinders in tandem, a phenomenon where the downstream cylinder suppresses vortex shedding from the upstream cylinder will occur at a critical T/d. This critical T/d will vary from 1.9 to 3.5 depending on Re (Zdravkovich 1977, 1987). The experiment carried out by Lam and Lo (1992) on four cylinders showed that the critical T/d occurred around 3.94 at $\mathrm{Re} = 2100$. In the present experiment where $\mathrm{Re} = 200$ the downstream cylinders are observed to be completely shielded by their upstream counterparts even at $T/d = 4$. This observation is consistent with the result of Lam and Lo (1992). It should be noted that the blockage ratio is 9.4% in their experiment and 13.3% in the present experiment, while the aspect ratios are 21.3 and 15, respectively. The slightly larger blockage in the present experiment could be one of the reasons why the critical T/d is marginally larger even though Re is much smaller. The question whether blockage will affect the shielding from the upstream cylinders is further explored in the following discussion.

Since cylinder 3 is completely shielded by the wake of cylinder 2, wake oscillations or boundary layer separations of cylinders 2 and 3 are in-phase, as are those on cylinders 1 and 4. The vortex shedding from cylinders 1 and 2 are anti-phase, which is the most common flow pattern of two cylinders in a side-by-side arrangement. Therefore, it can be inferred that the interference of vortex shedding is strong even at this large T/d and the flow pattern is different from that of two cylinders in tandem. The overall effect on the cylinders could be attributed to combination of proximity and wake interferences. During this experiment, in spite of the fact that the flow field was disturbed by swiftly accelerating or decelerating the incoming flow velocity, no change of shielding flow pattern to shedding flow pattern for cylinders 1 and 2 occurred. When compared with this experimental result, the two-dimensional (2D) computational results of Farrant et al. (2000) using a cell boundary method at $T/d = 3$ for $\mathrm{Re} = 200$ reveal shedding phenomena instead of shielding flow patterns behind the upstream cylinders. Moreover, their computational results showed that the shedding phenomenon led to a stronger fluctuating force on the upstream cylinders compared with that on an isolated cylinder. The lift amplitudes of cylinder 1 increased by approximately 25%, while those on the downstream cylinders were found to be many times larger. Lam et al. (2001) also failed to detect any shielding results from their calculations using a vortex method at the same T/d and Re.

Some attempts to calculate this bluff body flow have also been made using the 2D fluent commercial CFD software. In these calculations, unstructured grids were used and the flow field was initialized to be uniform and equal to the incoming flow. The numerical schemes were selected as follows: a second-order pressure scheme, a second-order upwind scheme for the convective term in the momentum equations, a segregated solver, and a SIMPLE scheme to treat the pressure and velocity coupling. A second-order implicit formulation was used to compute this periodic flow with a time step of 0.05 s. Among the attempts, several different computational domain sizes have been tried in order to evaluate the influence of wall blockage on the flow patterns. One domain has a size of 40 × 70 d, while the other two domains are of

$15 \times 70d$ and $15 \times 30\ d$, respectively, and have the same blockage as the present experimental set up. A smaller domain of $10 \times 70\ d$, which led to a larger blockage than the actual experiments, was also tested. Two different boundary conditions for the lateral side of the water tunnel, no slip wall condition and uniform free stream condition, have been examined. However, no shielding effect was found in the computational results. It appears that blockage is not the reason for the discrepancy between experiments and computations. Therefore, the prediction of the shielding flow pattern for this configuration represents a challenge to CFD.

The instantaneous flow field deduced from PIV measurements at $\alpha = 0^\circ$ is shown in Fig. 4 at an instantaneous time around $t/\tau = 0$. The vector plot clearly shows that the velocity of the gap flow is slightly higher and remains straight. The regions between the upstream cylinders and their downstream counterparts are enclosed by shear layers and are almost stagnated. The anti-phase flow pattern behind cylinders 3 and 4 is easily recognized from the streamline plot. The presence of the downstream cylinders suppressed vortex shedding from the upstream cylinders. As a result, vorticity is weak and vortices are shed immediately downstream behind cylinders 3 and 4.

3.2. *OVSA flow pattern—$\alpha = 15$*

With α increasing from 5° to 15°, the cylinder array looks like two rows of cylinders at a slightly staggered arrangement, and cylinders 3 and 4 are at a lower position compared with cylinders 2 and 1. In this range of α, every 5° variation would cause a distinctive change in the overall flow pattern. At $\alpha = 5^\circ$, although cylinder 1 still provides shielding for cylinder 4, the free shear layer on its lower side begins to touch the bottom of cylinder 4 from time to time before it curves back to form a vortex at the bottom side of cylinder 4. On the other hand, due to the effect of a high jet stream velocity in the gap, the free shear layer on the lower side of cylinder 2 reattaches on cylinder 3, and vortex sheds directly from the lower side of cylinder 3. When $\alpha = 10^\circ$, cylinders 3 and 4 are no longer shielded by cylinders 2 and 1. The flow pattern around cylinders 1 and 4 is similar to that around cylinders 2 and 3 at $\alpha = 5^\circ$, i.e., shear layer reattachment flow pattern. As for the flow around cylinders 2 and 3, the pattern is entirely different. The shear layers from both sides of cylinder 2 remain straight as they move downstream, before they are forced to move upward obliquely by the obstruction of cylinder 3. This causes the upper shear layer of cylinder 3 to move upwards. Therefore, the wake of cylinder 3 becomes wider and asymmetrical.

As α increases to 15°, noticeable changes occur, and the overall flow pattern is completely different (Fig. 5) from the fundamental pattern. At this configuration, for the first time, it was observed that two high-velocity confluent streams surround the nearly stagnated near wakes of cylinders 1 and 2. Therefore, the shear layers from both sides of these cylinders are tightly squeezed and cannot develop into mature vortices as in the case of a single cylinder, and their wakes can only oscillate slightly. Since cylinder 4 is nearer to cylinder 1 in the vertical direction than the others, the lower shear layer from cylinder 1 can only curve to form a very weak vortex and its wake is asymmetrical and oblique in the upward direction. Similarly, the presence of cylinder 3 downstream of cylinder 2 makes the wake of cylinder 2 asymmetrical and slanted in the upward direction, but this wake can oscillate freely. Just as in the case where $\alpha = 10^\circ$, the upper shear layer of cylinder 3 separates at similar angles. This causes the wake of cylinder 3 to be the widest among the four cylinders, so vortex shedding from cylinder 3 is clearly visible. Under the suppression of the gap flow between cylinders 3 and 4, the wake of cylinder 4 is not as wide as that of cylinder 3, although its upper shear layer also separates (see Fig. 5(b)). As there is no obvious vortex shedding from cylinder 1, so the synchronization between the lower shear layer of cylinder 1 and the upper shear layer of cylinder 4 is not distinct.

A closer examination of the vortices shed from both sides of cylinder 4 reveals two distinct features. First, the vortex formation of cylinder 4 is obviously shorter than that of a single cylinder. Second, the vortex shedding from its upper side is pushed into the core of its counterpart, then squeezed and stretched gradually downstream, and finally disappears. Meanwhile, vortex shedding from the lower side of cylinder 4 can keep its relatively round shape and grows continually larger, and embraces its counterpart. This flow pattern is very unique and occurs only in an array with at least three cylinders. Therefore, it is called OVSA, and this leads to the annihilation of one vortex row further downstream.

On the other hand, the flow interference between cylinders 2 and 3 involves the process of a vortex pairing and enveloping (VPE) flow pattern that is shown clearly in Fig. 5(a). A pair of vortices from cylinders 2 and 3 with opposite signs is pushed by the small gap flow bounded up by these two shear layers, then these pairing vortices run into the core of the vortex shedding from the outside of cylinder 2 and are enveloped. As a result, a composite vortex was formed. Sumner et al. (2000) explained in detail this VPE flow pattern. In the present experiment, it is believed that the high momentum flow in the gap is the cause of the VPE flow pattern.

The overall flow pattern at this α involves two basic flow patterns, OVSA and VPE. Since Sumner et al. (2000) has also observed the VPE, therefore, only the OVSA is a new pattern found in this study. Downstream of this array, only two rows of vortices are observed and they could seriously influence the structures further downstream. A structure

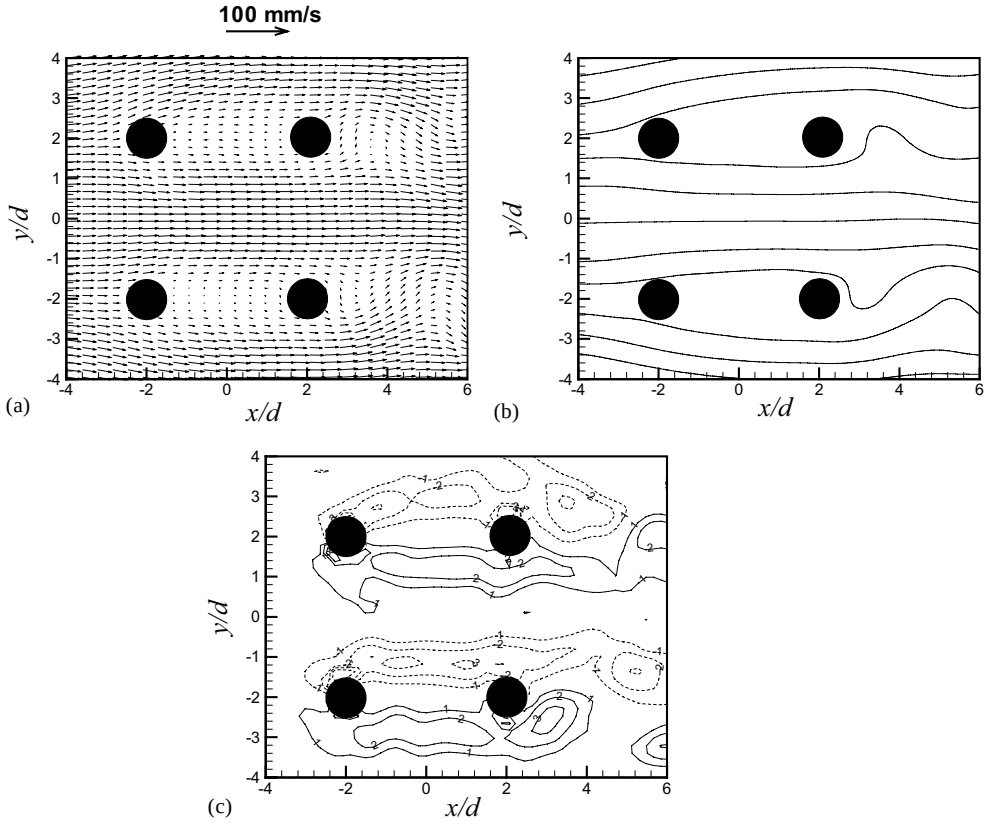

Fig. 4. Instantaneous in-plane flow field derived from PIV at $\alpha = 0^\circ$: (a) velocity field; (b) streamline field; and (c) vorticity field. Solid lines are positive vorticity levels and dashed lines are negative. Minimum and incremental contour levels are, respectively, 1 and $1\,s^{-1}$.

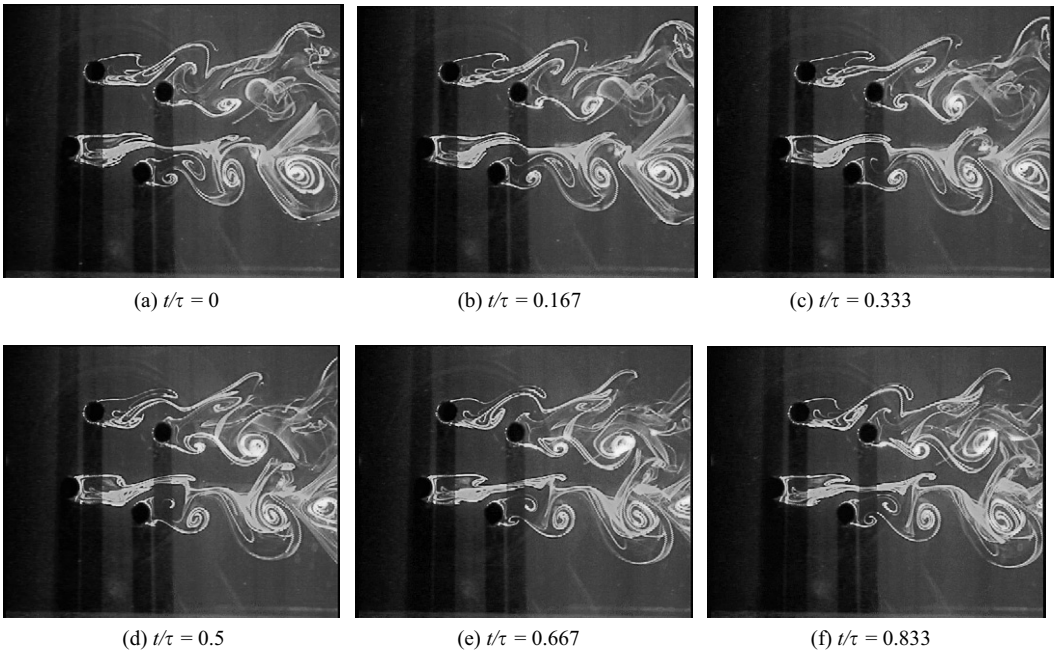

(a) $t/\tau = 0$ (b) $t/\tau = 0.167$ (c) $t/\tau = 0.333$

(d) $t/\tau = 0.5$ (e) $t/\tau = 0.667$ (f) $t/\tau = 0.833$

Fig. 5. Sequential photos of flow visualization at $\alpha = 15^\circ$.

downstream in the way of the composite vortex will experience fluctuating forces with higher frequency, while that in the way of the other rows of vortex will only be affected by forces with lower frequency, therefore the spectrum range of vortex-shedding frequency downstream of cylinder 3 will become wider and the prevention of resonance will become more difficult.

An instantaneous flow field corresponding to the flow pattern around $t/\tau = 0.833$ at $\alpha = 15^\circ$ derived from PIV is shown in Fig. 6. From the velocity map, it is clear that two separated nearly stagnated near wakes are formed behind cylinders 1 and 2. In addition, a relatively strong gap flow is formed before cylinder 3 and points at an oblique angle outward. The velocity of the gap flow is high compared with that of its neighbors. Thus, it appears as a narrow jet flow. This phenomenon is very prominent in the velocity map. A similar gap flow is also formed before cylinder 4, but it is directed downward immediately due to the stronger and wider major gap flow between cylinders 3 and 4. A close examination of the flow around cylinders 2 and 3 in Fig. 5 reveals that with the oscillation of the wake of cylinder 2, the direction and width of the jet before cylinder 3 change drastically, and this will give rise to a strong mean and fluctuating lift force on cylinder 3, so does cylinder 4. This inference is consistent with force measurements obtained in the separate experiment described above and with the data of Lam and Fang (1995). Therefore, this could be an important mechanism to generate large fluctuating force and mean lift force. Similar phenomena might also occur for two staggered cylinders in the range of VPE flow patterns. Furthermore, it is inferred that a little change of α could lead to an obvious change of mean lift force and this should be borne in mind in practical engineering design. The defined interference galloping by Ruscheweyh (1983) and Dielen and Ruscheweyh (1995) confirms the observation in the present study. Moreover, the fluctuating forces acting on cylinders 3 and 4 should be larger than those on cylinders 1 and 2 at this α, and the heat transfer ability of cylinders 3 and 4 will be more effective than other cylinders. The much wider wake of cylinder 3 is clearly shown in Fig. 6(b). From the vorticity map in Fig. 6(c), it can be seen that the vortex developed behind cylinder 4 consists of a negative one followed by a positive one along a single line. This in-line counter-rotating vortex pair leads to the squeezing of the negative vortex.

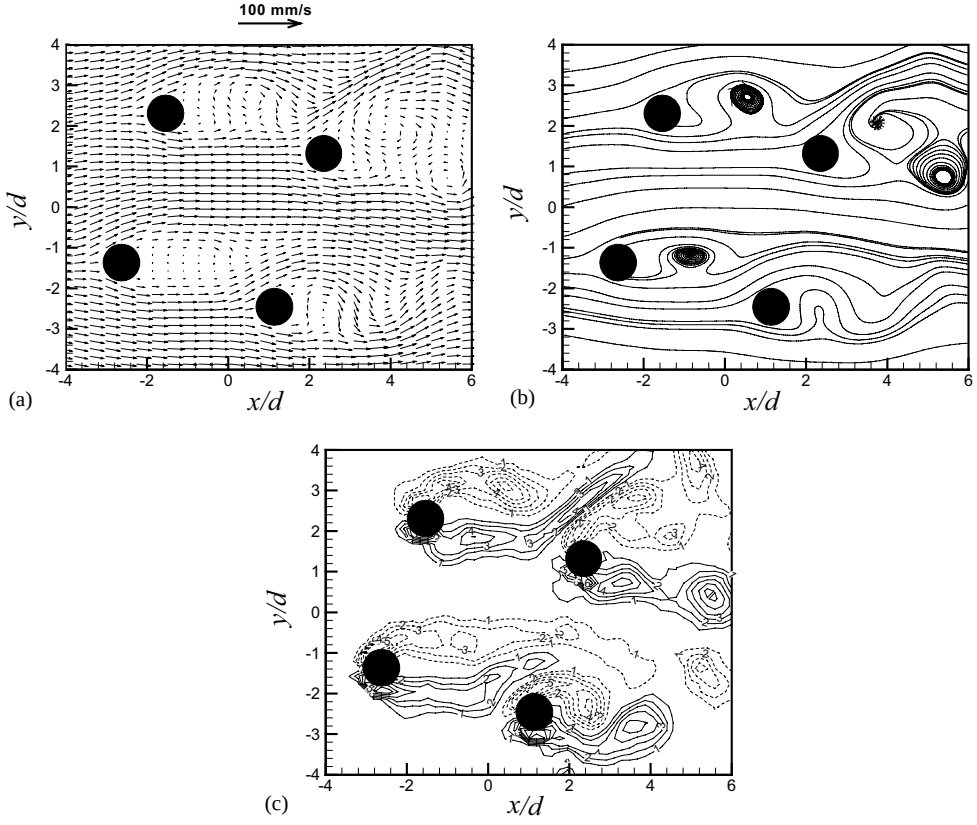

Fig. 6. Instantaneous in-plane flow field derived from PIV at $\alpha = 15^\circ$: (a) velocity field; (b) streamline field; and (c) vorticity field. Solid lines are positive vorticity levels and dashed lines are negative. Minimum and incremental contour levels are, respectively, 1 and 1 s^{-1}.

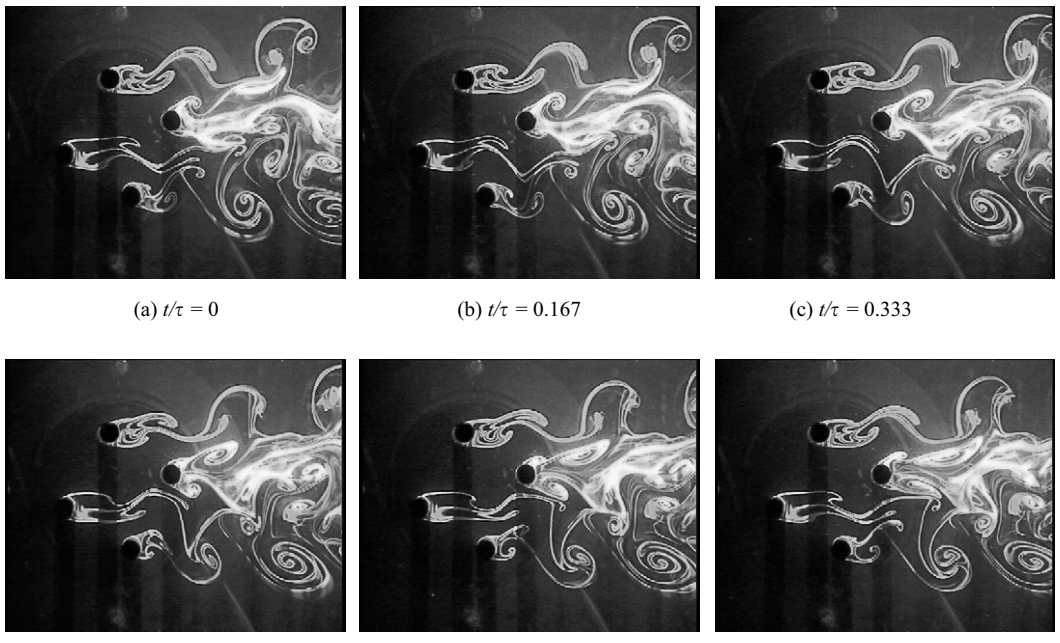

(a) $t/\tau = 0$ (b) $t/\tau = 0.167$ (c) $t/\tau = 0.333$

(d) $t/\tau = 0.5$ (e) $t/\tau = 0.667$ (f) $t/\tau = 0.833$

Fig. 7. Sequential photos of flow visualization at $\alpha = 30^\circ$.

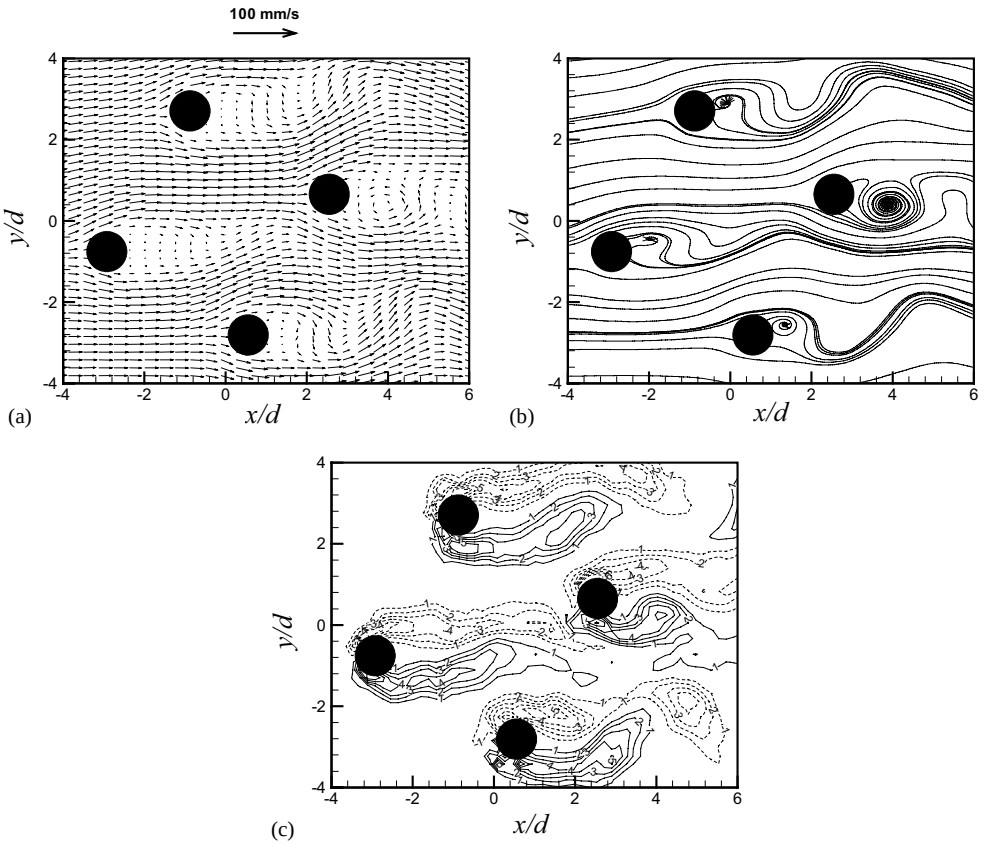

Fig. 8. Instantaneous in-plane flow field derived from PIV at $\alpha = 30^\circ$: (a) velocity field; (b) streamline field; and (c) vorticity field. Solid lines are positive vorticity levels and dashed lines are negative. Minimum and incremental contour levels are, respectively, 1 and 1 s^{-1}.

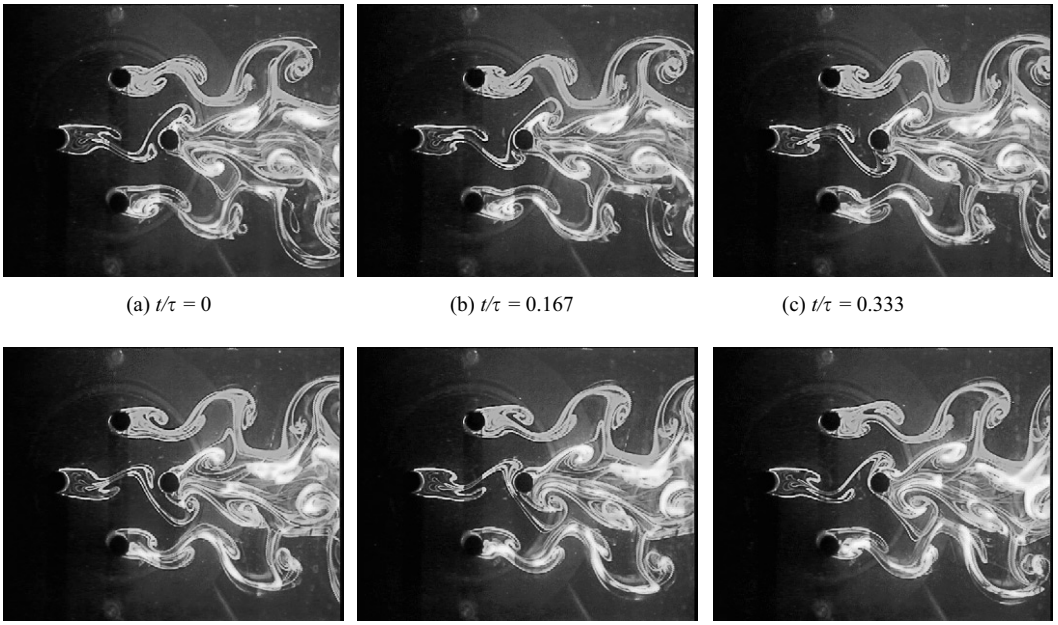

(a) $t/\tau = 0$ (b) $t/\tau = 0.167$ (c) $t/\tau = 0.333$

(d) $t/\tau = 0.5$ (e) $t/\tau = 0.667$ (f) $t/\tau = 0.833$

Fig. 9. Sequential photos of flow visualization at $\alpha = 45^\circ$.

3.3. *VPRP flow pattern—$\alpha = 30^\circ$*

In the range of $\alpha = 20-35^\circ$, the overall flow patterns are quite similar. Compared with those described above, several evident changes are noticeable. Firstly, the wake interference of cylinder 1 on cylinder 4 decreases, but this wake gradually affects cylinder 3. Secondly, every cylinder is exposed to the main stream more directly and four separated and nearly stagnation regions are formed behind each cylinder. Therefore, the gap flow between the wake of cylinder 2 and the front surface of cylinder 3 becomes wider and stronger than before, and the flow angle becomes less tilted upward. Meanwhile, the oscillation of the jet width and angle decreases. This leads to a decrease of the mean and fluctuating lift force acting on cylinders 3 and 4.

The LIF flow visualization result at $\alpha = 30^\circ$ shown in Fig. 7 is a representative flow pattern in this α range. Compared with that at $\alpha = 15^\circ$, the first major change observed is the disappearance of the VPE flow pattern between cylinders 2 and 3 beyond $\alpha = 20^\circ$. Instead, the vortex shedding from the lower side of cylinder 2 synchronizes with the vortex from the upper side of cylinder 3 and forms a counter-rotating vortex pair. Unlike the gap VPE flow pattern found in Sumner et al. (2000) for the flow around two staggered cylinder array, the upper shear layer of cylinder 2 has already curled up and formed a small vortex before this vortex pair reaches its core. Therefore, these pairing vortices and the single vortex make up a new composite pairing vortices in the end. This flow pattern involves a VPRP and is a new feature for this configuration. It is designated as a VPRP flow pattern.

The most commonly observed flow pattern for two staggered cylinders is synchronized vortex shedding (SVS). In this range of α, the general features of this flow pattern change slightly. First of all, since cylinder 3 is located downstream of cylinders 1 and 2, its vortex shedding is synchronized with the shear layers of cylinders 1 and 2, therefore, both shear layers separate alternatively and two pairing vortices appear. This leads to a wide and nearly symmetrical wake. Also, the pairing vortices between cylinders 2 and 3 may develop into a VPRP flow pattern under this configuration or into a VPE flow pattern at $\alpha = 15^\circ$or 20°. In contrast, as cylinder 1 is located between and in front of cylinders 3 and 4, its upper and lower shear layers first synchronize with cylinders 3 and 4 in an alternate manner, and then form two pairing, counter-rotating vortices. However, its wake is rather narrow compared with that of cylinder 3. This SVS on both sides and pairing (SVSBP) flow pattern can be clearly observed in the middle of Fig. 7(e) and can only occur in arrays with at least three cylinders. It is also a popular flow pattern in this α range.

With increasing α, the gap flow before cylinder 4 becomes wider and wider, while the flow beneath cylinder 3 become narrower and narrower. Therefore, this leads to a bigger and bigger vortex formation by the upper shear layer of cylinder 4 and a smaller and smaller vortex formation by the lower shear layer of cylinder 3. Due to the change of gap

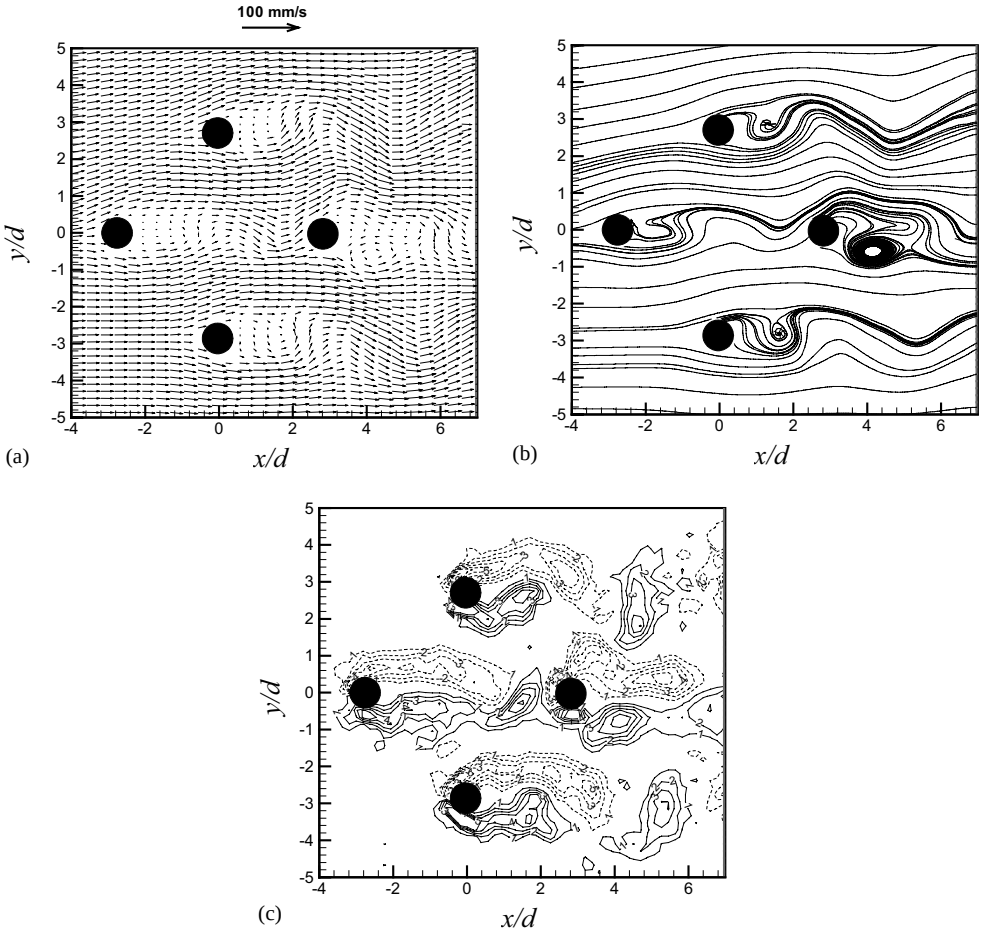

Fig. 10. Instantaneous in-plane flow field derived from PIV at $\alpha = 45°$: (a) velocity field (b) streamline field; and (c) vorticity field. Solid lines are positive vorticity levels and dashed lines are negative. Minimum and incremental contour levels are, respectively, 1 and $1\,s^{-1}$.

flows below cylinder 3 and above cylinder 4, the strength and sizes of the two pairing vortices change accordingly. Moreover, under the induction and obstruction of the pairing vortices and others around them, the motion and path of these two pairing vortices is rather complicated and are very sensitive to the orientation of the configuration. Structures just in the way of the two vortex pair will experience the higher frequency of the fluctuating forces and their multiples than that caused by normal vortex shedding. For cylinder 4, its lower shear layer begins to roll up almost at the separation point and grows into a large circular vortex quickly. Consequently, any downstream structures will experience dynamical forces at the vortex-shedding frequency; this is different from those downstream of cylinder 3.

Fig. 8 presents an instantaneous velocity field around $t/\tau = 0.667$ derived from PIV measurements at $\alpha = 30°$. Compared with the velocity map and streamlines distribution at $\alpha < 20°$, it can be seen that the gap flow above cylinder 4 becomes wider and stronger. On the other hand, the gap flow beneath cylinder 3 is narrower and weaker. This is the reason why the vortex from the upper side of cylinder 4 can develop into a big one. Moreover, the flow around cylinders 3 and 4 is almost symmetrical. This implies that the lift force acting on them should be approximately zero. Since the vorticity map clearly shows that the shear layer from cylinder 1 is almost in contact with the vortex from cylinders 3 and 4 directly, this leads to a strong interaction and a possible synchronization among the vortices.

From the above discussion, it is clear that the SVSBP flow pattern is the most "popular" one among three-cylinder arrays. Its development is very sensitive to the orientation of the cylinders. Therefore, the structures downstream may experience multiple Strouhal numbers. Similar process might happen in tube arrays. For example, Fitzpatrick et al. (1988) found that a similar phenomenon happened in a triangular-type array but could not explain the reason. In other air and water flow experiments, Price et al. (1987) found that three dominant Strouhal numbers inter-related in the

ratios 1:2:3 exist in the interstitial flow in several of the upstream rows. The present study shed light on these phenomena and provides reasonable explanations for their appearance.

3.4. VIIS flow pattern—$\alpha = 45^\circ$

When $\alpha = 40^\circ$ or 45°, cylinder 3 is almost directly downstream of cylinder 1. Therefore, vortex shedding from cylinder 1 impinges on cylinder 3 directly, and a VI flow pattern will occur. Since the direction and magnitude of the oncoming flow on cylinder 3 change rapidly, it is reasonable to infer that the vortex–structure interaction will cause large changes in the time-dependent pressure forces and loading on the downstream cylinder, thus, significantly enhancing the root mean square (r.m.s.) values of the fluid force coefficients acting on the downstream cylinder.

At $\alpha = 40^\circ$, only one row of vortices shed from cylinder 1 impinges on cylinder 3, and then it splits; one part causes the shear layer on the upper side of cylinder 3 to separate immediately, thus giving rise to a new vortex. However, the other part with an opposite sign vorticity suppresses vortex formation from the lower side of cylinder 3, and causes its shear layer to separate. This behavior leads to a complex and asymmetric wake for cylinder 3. The vorticity map clearly shows that the vorticity strength on the upper side of cylinder 3 is larger and more regular than its lower side.

At $\alpha = 45^\circ$, the configuration gives a pure diamond shape as shown in Fig. 9. Contrast this flow pattern to that at $\alpha = 0^\circ$, the free shear layers of cylinder 1 do not develop long enough to shield the downstream cylinder 3; instead they begin to roll up very soon (approximately $1.5d$ behind cylinder 1). The SVSBP flow pattern occurs among cylinders 1, 2 and 4 and cylinders 2, 3 and 4, and their vortex shedding are the most popular anti-phase pattern. It is very interesting to note that although cylinders 2 and 4 are in a side-by-side arrangement, with the presence of cylinder 1 or 3 in the middle, their vortex shedding becomes in-phase. On the other hand, cylinders 1 and 3 are in tandem, therefore, the vortex shed from cylinder 1 impinges on cylinder 3 alternately. When the vortex from cylinder 1 strikes on the front surface of cylinder 3, it will immediately slide past its surface. With the arrival of a strong vortex having the same sign, the shear layers of the downstream cylinder separate without the formation and roll-up of a free shear layer like the Karman vortex formation. Thus, the wake of cylinder 3 is widest among the four cylinders and its shape is symmetrical with alternating vortex shedding behind it. This VIIS flow pattern is different from the VI flow pattern observed at $\alpha = 40^\circ$.

Comparing the forces measured on cylinders 3 and 4 at $\alpha = 45^\circ$ and 15° in a separate force measurement experiment, it is found that the r.m.s. fluctuating forces at the $\alpha = 15^\circ$ arrangement are larger in magnitude, so are the mean lift forces. On the other hand, the drag force on cylinders 3 and 4 at $\alpha = 45^\circ$ are at a minimum and a maximum, respectively.

The velocity field at $\alpha = 45^\circ$ shown in Fig. 10 can help to explain the differences noticed in the measured forces. The velocity field corresponds to the flow pattern around $t/\tau = 0$ is shown in Fig. 9. From the velocity map, it can be seen that the flow field around cylinders 1, 2 and 4 are close to that of a single cylinder, while cylinder 3 is directly in the wake of cylinder 1. However, at $\alpha = 15^\circ$ almost half of cylinders 3 and 4 are immersed in the low-pressure wake of their upstream counterparts, therefore, they will experience larger mean lift forces and moderate mean drag forces. Due to the formation of the narrow high-speed gap flow before cylinders 3 and 4 at $\alpha = 15^\circ$, the velocity becomes higher than that before cylinder 3 at $\alpha = 45^\circ$ at one instant and become lower at another instant when the nearly stagnated wake oscillates. Therefore, the variation of the direction and magnitude of the gap flow can be more serious under the influence of the oscillation of the near wake than that at this diamond configuration (by comparing the oscillation of the free shear layers or streak lines of cylinder 3), this lead to stronger fluctuating forces. From the streamline map, the in-phase vortex-shedding pattern between cylinders 2 and 4 is quite obvious. Furthermore, the vorticity map clearly shows the VI flow pattern, and the vortex formation on the bottom side of cylinder 3 is apparent. Due to the induction of the incoming vortex, the vortex formation length of cylinder 3 is short compared with that of other configurations. This result is consistent with the observation from flow visualization.

4. Conclusions

In this study, the wake patterns and flow fields of four cylinders arranged in a square configuration under steady laminar uniform cross-flow were investigated using a laser-induced fluorescent (LIF) visualization technique and a particle image velocimetry (PIV) technique. The Reynolds number, Re, is 200 based on the oncoming flow and the diameter of the individual cylinders. The spacing ratio T/d is set at 4 and the cylinder configuration can be rotated to give different angles of attack α. Altogether, 10 different α values, ranging from 0°–45°, were investigated and a detailed flow pattern for each α was obtained. From these results, distinctive features of the flow pattern at the configurations investigated are summarized below.

(i) There exist four basic groups of flow around a four-cylinder array. The first is a fundamental group occurring only at $\alpha = 0^\circ$. The second flow group is found in array configurations with α varying from 5° to 15°. In this α range, a very small change in α, or direction of the oncoming flow, will give rise to a very different flow pattern (from shielding effect to jet-flow effect), and therefore lead to a large change in the mean and fluctuating lift and drag forces. This would cause serious lift reversal, vibration and even damage to the structures. The third group spans an α range from 20° to 35°. At these α values, vortex pairings and their development lead to the interference of vortex shedding with the moving free vortices. As a result, the wakes of the cylinders are very complicated and are sensitive to α. The fourth group covers α ranging from 40° to 45°. Within this α range, vortex impingement (VI) and VI with induced separation are the main features of these flow patterns; therefore, the fluctuating force acting on cylinder 3 is large and could lead to serious vibration on cylinder 3.

(ii) With the exception of the first group, new flow patterns were observed in the other three groups. The new flow patterns for group 2 to 4 are designated, respectively, as opposite vortex squeezing and absorbing flow pattern (OVSA), vortex pairing and repairing flow pattern (VPRP), and vortex impingement and induced separation flow pattern (VIIS). Some of these flow patterns only occur among multi-cylinders and were not observed for two staggered cylinders. These flow patterns have not been reported previously.

(iii) From the flow visualization results, it was found that the SVSBP flow pattern that is the most popular interference pattern in a three-cylinder array is also found in the α range where VPRP flow pattern occurs. Moreover, these pairing vortices are very sensitive to the flow condition around the cylinders and can develop into different flow patterns, such as VPE, VPRP, etc. Hence, the structures downstream might experience multiple Strouhal numbers, and usually these Strouhal numbers are in harmony.

(iv) Two major flow patterns, which give rise to strong fluctuating forces and serious vibration, are observed in this experiment. One major flow pattern is the impingement by an oncoming vortex directly, such as that observed in cylinder 3 at $\alpha = 45^\circ$. The other is the formation of a jet flow between the relatively stagnated wake of the upstream and downstream cylinder. Such a jet flow is also observed at the configuration given by $\alpha = 15^\circ$. This jet flow is different from the ordinary gap flow, its velocity is high and its width is narrow. So, a small change in the shape of the wake will lead to a large change in the direction and magnitude of the jet. This behavior could lead to serious structural vibrations and should be noted in practical engineering applications.

Acknowledgements

This work was fully supported by a grant from the Research Grants Council of the Hong Kong Special Administrative Region, China (Project No. PolyU 5147/99E).

References

Bearman, P.W., Wadcock, A.J., 1973. The interaction between a pair of circular cylinders normal to a stream. Journal of Fluid Mechanics 61, 499–511.

Dielen, B., Ruscheweyh, H., 1995. Mechanism of interference galloping of two identical circular cylinders in cross flow. Journal of Wind Engineering and Industrial Aerodynamics 54/55, 289–300.

Farrant, T., Tan, M., Price, W.G., 2000. A cell boundary element method applied to laminar vortex-shedding from arrays of cylinders in various arrangements. Journal of Fluids and Structures 14, 375–402.

Fitzpatrick, J.A., Donaldson, I.S., Mcknight, W., 1988. Strouhal numbers for flows in deep tube array models. Journal of Fluids and Structures 2, 145–160.

Gu, Z.F., 1996. On interference between two circular cylinders at supercritical Reynolds number. Journal of Wind Engineering and Industrial Aerodynamics 62, 175–190.

Gu, Z.F., Sun, T.F., 1999. On interference behind two circular cylinders in staggered arrangement at high subcritical Reynolds numbers. Journal of Wind Engineering and Industrial Aerodynamics 80, 287–309.

Guillaume, D.W., Larue, J.C., 1999. Investigation of the flopping regime with two-, three- and four-cylinder arrays. Experiments in Fluids 27, 145–156.

Kareem, A., Kijewski, T., Lu, P.C., 1998. Investigation of interference effects for a group of finite cylinders. Journal of Wind Engineering and Industrial Aerodynamics 77&78, 503–520.

Lam, K., Cheung, W.C., 1988. Phenomena of vortex shedding and flow interference of three cylinders in different equilateral arrangements. Journal of Fluid Mechanics 196, 1–26.

Lam, K., Fang, X., 1995. The effect of interference of four equispaced cylinders in cross flow on pressure and force coefficients. Journal of Fluids and Structures 9, 195–214.

Lam, K., Lo, S.C., 1992. A visualization study of cross-flow around four cylinders in a square configuration. Journal of Fluids and Structures 6, 109–131.

Lam, K., So, R.M.C., Li, J.Y., 2001. Flow around four cylinders in a square configuration using surface vorticity method. Proceedings of the Second International Conference on Vortex Methods, Turkey, pp. 115–122.

Liu, Y., So, R.M.C., Lau, Y.L., Zhou, Y., 2001. Numerical studies of two side-by-side cylinders in a cross flow. Journal of Fluids and Structures 15, 1009–1030.

Ng, C.W., Ko, N.W.M., 1995. Flow interaction behind two circular cylinders of equal diameter—a numerical study. Journal of Wind Engineering and Industrial Aerodynamics 54/55, 277–287.

Price, S.J., Paidoussis, M.P., 1984. The aerodynamic forces acting on groups of two and three circular cylinders when subjected to a cross flow. Journal of Wind Engineering and Industrial Aerodynamics 17, 329–347.

Price, S.J., Paidoussis, M.P., Macdonald, R., Mark, B., 1987. The flow-induced vibration of a single flexible cylinder in a rotated square array of rigid cylinders with pitch-to-diameter ratio of 2.12. Journal of Fluids and Structures 1, 359–378.

Ruscheweyh, H., 1983. Aeroelastic interference galloping effects between slender structures. Journal of Wind Engineering and Industrial Aerodynamics 14, 129–140.

Sayers, A.T., 1988. Flow interference between four equispaced cylinders when subjected to a cross flow. Journal of Wind Engineering and Industrial Aerodynamics 31, 9–28.

Sayers, A.T., 1990. Vertex shedding from groups of three and four equispaced cylinders situated in a cross flow. Journal of Wind Engineering and Industrial Aerodynamics 34, 213–221.

So, R.M.C., Liu, Y., Zhou, Y., 2000. Fluid–structure interactions of two side-by-side circular cylinders. In: Ziada, S., Staubli, T. (Eds.), Flow-Induced Vibration Proceedings of the Seventh International Conference on Flow Induced Vibrations FIV 2000, A. A. Balkema, Rotterdam, Netherlands, pp. 97–103.

Sumner, D., Wong, S.S.T., Price, S.J., Paidoussis, M.P., 1999. Fluid behavior of side-by-side circular cylinder in steady cross-flow. Journal of Fluids and Structures 13, 309–338.

Sumner, D., Price, S.J., Paidoussis, M.P., 2000. Flow-pattern identification for two staggered circular cylinders in cross-flow. Journal of Fluid Mechanics 411, 263–303.

Tatsuno, M., Amamoto, H., Ishi-I, K., 1998. Effects of interference among three equidistantly arranged cylinders in a uniform flow. Fluid Dynamics Research 22, 297–315.

Ting, D.S.-K., Wang, D.J., Price, S.J., Paidoussis, M.P., 1998. An experimental study on the fluid elastic forces for two staggered circular cylinders in cross-flow. Journal of Fluids and Structures 12, 259–294.

Zdravkovich, M.M., 1968. Smoke observation of the wake of a group of three cylinders in various arrangements. Journal of Fluid Mechanics 32, 339–351.

Zdravkovich, M.M., 1977. Review-review of flow interference between two circular cylinders in various arrangements. ASME Journal of Fluids Engineering 99, 618–633.

Zdravkovich, M.M., 1987. The effects of interference between circular cylinders in cross flow. Journal of Fluids and Structures 1, 239–261.